PAPER

Check for updates

DFT and solvent-phase insights into nitrosourea adsorption on AlN, GaN and their in-plane heterostructure (AlN/GaN) nanosheets

Tabassum Yesmin Saba, Afiya Akter Piya, [ID] * Tanvir Ahmed and Siraj Ud Daula Shamim [ID]

Cancer is the second most common cause of death worldwide and its frequency is rising as the population grows. Nanotechnology has become a viable strategy for targeted cancer therapy in order to overcome these constraints in drug delivery. This study focuses on the adsorption behavior, electrical characteristics and drug–carrier interactions of the anticancer drug nitrosourea (NU) with pristine aluminum nitride (AlN) and gallium nitride (GaN) nanosheets along with their in-plane heterostructures (AlN/GaN (H1) and GaN/AlN (H2)) as efficient and selective potential nanocarriers for the delivery using density functional theory (DFT) in both air and water media. Our calculations showed that the NU adsorbed on AlN, AlN/GaN (H1), GaN and GaN/AlN (H2) with adsorption energies of −0.94, −0.74, −0.72, and −0.64 eV in air media and −0.75, −0.76, −0.51, and −0.36 eV in water media for the most stable complexes, respectively. After adsorption, the HOMO–LUMO energy gaps were reduced to be 3.84 to 1.87, 3.54 to 1.15, 3.37 to 2.07 and 3.54 to 2.18 eV for these nanosheets. The reduced HOMO–LUMO energy gap enhances the conductivity of the nanosheets and improved their applicability for electronic drug detection. The increased dipole moments and work function changes, mainly in water media following NU adsorption, indicate improved polarity and solubility. Furthermore, reactivity and stability were assessed using Conductor-like Screening Model (COSMO) surface and quantum molecular descriptor studies. According to our research, AlN and GaN based nanomaterials showed great promise as effective and selective NU carriers. Among them AlN in state 2 indicated their potential as effective nanocarriers for nitrosourea by exhibiting the best adsorption energy, electronic modulation and structural integrity.

1. Introduction

Cancer is the most typical cause of death globally, out of all the life-threatening and incurable diseases. Cancer is the world's second leading cause of death. Cancer claims many lives each year. Due to the ongoing global population growth, the number of new cases is increasing every day. An estimated 20 million new instances of cancer and 10.3 million cancer-related deaths are expected worldwide in 2025.[1] Cancer develops due to the uncontrolled growth of abnormal cells. One of the most crucial stages in evaluating cancer is the lack of cell cycle control. Cancer arises when the unregulated growth of invading cells spreads to other parts of the body.[2] Human cancer is a genetic disease that can often be associated with specific alterations in growth-promoting gene or tumor suppressor gene expression.[3] The TCGA Research Network published an interim analysis of 3527 tumors from 12 distinct cancer types in 2014.[4] Carcinomas, sarcomas, leukemia, lymphomas, breast cancer and throat cancer are the six primary forms.[5] Depending on the type and stage of

Department of Physics, Mawlana Bhashani Science and Technology University, Tangail-1902, Bangladesh. E-mail: afiya@mbstu.ac.bd

cancer, there are many ways to treat it.[6] Cancer can be treated by radiation therapy, chemotherapy, surgery, immunotherapy and targeted therapies.[7] Chemotherapy is usually seen to be a powerful way to treat cancer. But it can have serious harmful effects since it might kill healthy cells or tissues.[8] Radiation therapy method of cancer treatments makes use of high doses of radiation generally ionizing radiation to kill cancer cells and destroy the tumor tissues.[9] Surgery is frequently used to treat cancer. Especially used for non-hematological tumors.[10] Anti-cancer drugs are the main category of therapeutic substances that can be applied.[11] One well-known simple organic molecule that is essential to cancer chemotherapy is nitrosourea.[12] Nitrosourea (NU) belongs to a class of cancer drug known as alkylating agents which work by blocking DNA repair through the alkylation process.[13] NU can penetrate the blood–brain barrier and is used to treat brain tumors. Nitrosourea is currently used to treat psoriasis,[14] essential thrombocythemia,[15] HIV infection,[16] leukemia,[17] sickle cell anemia[18,19] and polycythemia vera *etc.* Nanotechnology provides effective and promising methods for treating cancer.[20] Structures that are approximately 1 to 100 nm in size in at least one dimension are referred to as nanotechnology.[21] Tumor targeting is one of the potential core benefits of using

nanotechnology to treat cancer. One of the main goals of nanotechnology in the treatment of cancer is the capacity to distinguish between cancerous and nonmalignant cells and to eliminate cancerous cells only.[22] Nanotechnology has the advantages of lowering adverse effects, increasing drug accumulation at tumor locations and enabling controlled and prolonged drug release.[23] The inability of standard chemotherapy to target cancer results in damaging effects on healthy cells as well as serious side effects as nausea, vomiting, acidity and appetite loss.[24]

To reduce adverse effects of drugs, nanomaterials are used in drug delivery. Different kind of nanomaterials are used for drug-delivery purposes such as zero-dimensional (0D), one-dimensional (1D), two-dimensional (2D) and three-dimensional (3D) materials. Among them, 2D nanomaterials exhibit remarkable electric and thermal conductivity, as well as high surface ratio, carrier mobility, and solubility.[25] The intriguing characteristics and extensive range of uses of graphene-based 2D nanomaterials have drawn the interest of researchers.[26] One of the best methods to increase graphene nanosheets reactivity is by doping. Certain cells can be targeted by conjugating AlN and GaN nanostructures. They are appropriate for drug delivery due to their chemical and thermal resistance.[27] In earlier studies, researchers enhanced graphene nanosheets by incorporating nitrogen (N) and aluminum (Al) atoms to form heterostructures. It was discovered that the addition of heteroatoms enhanced the nanosheets interaction behavior. Kassaee et al. investigated the sensing behavior of the bendamustine drug by AlN and GaN was also considered as a drug carrier in the drug delivery system.[28] By using DFT to investigate the detection of bendamustine on AlN and Si-doped C nanocones and nanosheets, Ayoubi-Chianeh et al. discovered that AlN nanosheets shown promise as a bendamustine drug sensor.[29] Louis et al. also used DFT to investigate heteroatom (B, N, S)-doped graphene quantum dots as a possible drug delivery system for isoniazid and found that the doped graphene exhibited a significant interaction with the drug.[30]

Our aim is to identify some suitable nanosheets as a carrier for nitrosourea and in this regard we calculated adsorption energy of AlN, AlN/GaN (H1), GaN and GaN/AlN (H2) based on DFT method. To increase the selectivity of NU as well as its reactivity, AlN and GaN nanosheets and their in-plane heterostructures nanosheets were investigated. To analyze the adsorption behavior of the proposed nanomaterials towards NU drug adsorption energy, adsorption distance, charge transfer, the dipole moment, HOMO and LUMO energy, energy gap, solvent energy, drug release time, work function, density of states (DOS) and partial density of states (PDOS) were investigated to understand the electronic properties of both the air and water media. Moreover, we conducted a COSMO surface analysis and quantum molecular descriptors to analyze the reactivity of the suggested nanomaterials toward NU.

2. Computational details

In this investigation, the spin-unrestricted DFT framework in the DMol3 module was used for all calculations in both air and water media.[31,32] In order to optimize the structures of the

nanosheets and the complexes of NU,[33] generalized gradient approximation (GGA) was selected in place of local density approximation (LDA), as it has been demonstrated in a number of previous studies that LDA inflates results for the equilibrium distance and bond energy.[34] Using Grimme dispersion-corrected Perdew–Burke–Ernzerhof (PBE), the van der Waals interactions with a long-range electron effect were observed.[35] Additionally, the DFT semi-core pseudopotential with a double-numerical basis set with polarization (DNP) was used in the core treatment since it was more accurate than the 6-31G (d, p) basis set in Gaussian.[36,37] Based on the DNP basis set, the basis set superposition error (BSSE) can be reduced or even eliminated.[38] A water medium with a dielectric constant of 78.54 was employed to investigate the solvent effect of the nanosheets and complexes.[39] The global orbital cutoff radius was 5 Å. The COSMO method was used to predict the solvent effect.[40]

The adsorption energy (E_{Ad}) of the nanosheets toward the anti-cancer drug NU was determined in our study using the following formula:[41]

$$E_{Ad} = E_{NU/nanosheets} - E_{nanosheets} - E_{NU} \tag{1}$$

where, $E_{NU/nanosheets}$, $E_{nanosheets}$ and E_{NU} are the total energies of the complexes, nanosheets and the NU molecule respectively.

The frontier molecular orbital (FMO) analysis, i.e., of the highest occupied molecular orbital (HOMO) and lowest unoccupied molecular orbital (LUMO) was performed and the energy gap (E_g) between the HOMO and LUMO was computed as follows,

$$E_g = E_{LUMO} - E_{HOMO} \tag{2}$$

where, E_{HOMO} and E_{LUMO} are the energy of the HOMO and the energy of the LUMO respectively.

Quantum molecular descriptors such as the chemical potential (μ), global hardness (η), global softness (S), electrophilicity (ω) and nucleophilicity (ν) index were also calculated to predict the reactivity of the nanosheets toward NU by the following equations,

$$\text{Chemical potential, } \mu = -(E_{HOMO} + E_{LUMO})/2 \tag{3}$$

$$\text{Global hardness, } \eta = (E_{LUMO} - E_{HOMO})/2 \tag{4}$$

$$\text{Global softness, } S = 1/2\eta \tag{5}$$

$$\text{Electrophilicity index, } \omega = \mu^2/2\eta \tag{6}$$

$$\text{Nucleophilicity index, } \eta = 1/\omega \tag{7}$$

COSMO with a dielectric constant of 78.54 was used to investigate the interaction between NU and the nanosheets in a water media.

3. Results and discussion

3.1 Geometry of optimized nanosheets

For this investigation, AlN and GaN nanosheets as well as their in-plane heterostructures were taken as drug carriers. Two
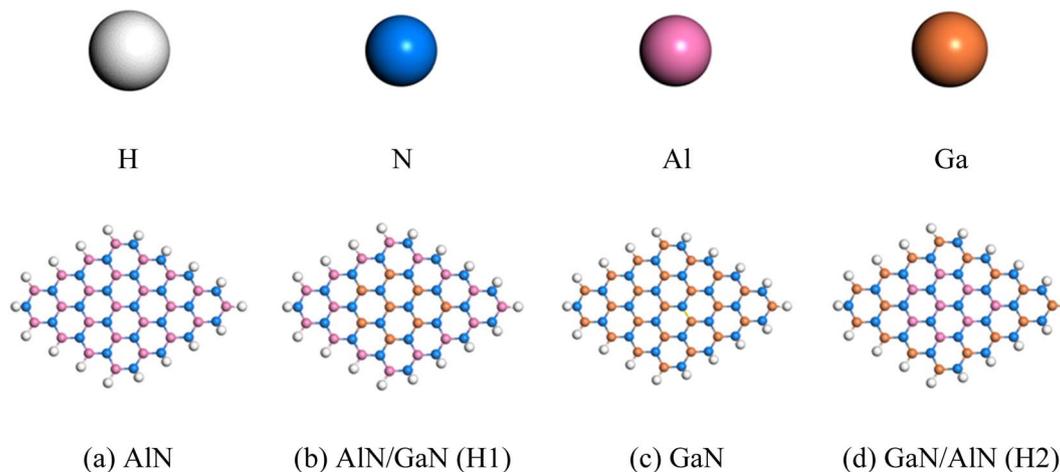
Fig. 1 (a–d) Top view of the optimized pristine and their in-plane heterostructures nanosheets.

pristine and two in-plane heterostructures nanosheets were evaluated as drug carriers for NU drug. The pristine AlN nanosheet was changed by heterostructures GaN at the central region. After the modification, all of the nanosheets were optimized at the ground state, as shown in Fig. 1. Each nanosheet consists of 66 atoms. The 48 carbon atoms in the AlN nanosheet employed in this work were passivated with hydrogen atoms at their edges to increase their stability.[2] In AlN, the average bond length between C and C was 1.54 Å, the bond length between C and H was 1.09 Å and the bond length between C and N was 1.47 Å. Furthermore, the C–C–C and C–C–H bond angles in AlN were 120.09° and 118.85° when GaN were used to in-plane heterostructures AlN.[42]

The bond lengths of Al–N in AlN and Ga–N in GaN were determined to be 1.812 and 1.843 Å, respectively. The nanosheets exhibit semiconducting behavior with energy gap 3.84, 3.37, 3.54 and 3.54 eV for AlN, GaN, AlN/GaN and GaN/AlN respectively visualized in DOS spectra displayed in Fig. 2. The thermodynamic stability of the nanosheets were confirmed by vibrational frequency analysis and the Gibbs free energy. All the nanosheets show positive vibrational modes with the minimum vibrational frequencies, 99.2, 87.1, 66.7 and 70.4 cm^{-1} and highest vibrational frequencies 3519.7, 3514.6, 3538.5, and 3540.4 cm^{-1}, for AlN, AlN/GaN (H1), GaN, and GaN/AlN (H2) respectively. All the positive modes indicate the dynamic stability of the four nanosheets. The calculated Gibbs free energies of the AlN, AlN/GaN (H1), GaN, and GaN/AlN (H2) are −58.269, −62.839, −71.087 and −67.266 kcal mol^{-1}, respectively. The negative values of Gibbs free energies confirmed the thermodynamics stability of the four nanosheets.

3.2 Adsorption of NU on the pristine and their in-plane heterostructures of AlN and GaN

In order to optimize all of the complexes, we arranged NU in parallel on the nanosheets of states 1 (S_1), NU with H atom toward the nanosheets of states 2 (S_2) and NU with O atom toward the nanosheets of states (S_3). All the configurations were relaxed in ground states and optimized structures are shown in Fig. 3. After optimization, we calculated adsorption energies by

using eqn (1), minimum adsorption distances and charge transfer and tabulated in Table 1. A negative interaction energy was found which suggesting that an exothermic and attractive interaction between the nanosheets and the NU.[43] In states 1, the adsorption energy of AlN, AlN/GaN (H1), GaN and GaN/AlN (H2) is −0.59, −0.74, −0.63, and −0.64 eV in the air media. All nanosheets show high range physisorption interaction with the NU drug. Among them, H1 structure shows highest interaction for S1 configuration.

In case of water media for S1, the calculated adsorption energies are −0.67, −0.76, −0.39, −0.36 eV for AlN, AlN/GaN (H1), GaN and GaN/AlN (H2). For state 2, the adsorption energies of AlN, AlN/GaN (H1), GaN and GaN/AlN (H2) nanosheets are −0.94, −0.18, −0.72 and −0.24 eV in air media and −0.75, −0.05, −0.51 and −0.19 eV in water media, respectively. In this case, the pristine AlN and GaN in both air media and water media exhibited favorable interaction energy with NU drug. In state 3, the adsorption energies of pristine AlN, AlN/GaN (H1), GaN and GaN/AlN (H2) nanosheets were −0.46, −0.41, −0.43 and −0.23 eV in air media and −0.54, −0.56, −0.37 and −0.22 eV in water media, respectively. In this case, the pristine AlN in air media and AlN/GaN (H1) water media exhibited favorable interaction energy with NU drug.

During the interaction with NU, Hirshfeld charge analysis was considered and calculated by the following equation,

$$\text{Charge transfer, } Q = Q_a \text{ (NU)} - Q_b \text{ (NU)} \tag{8}$$

where, the net charge on NU is denoted by Q_a (NU) and Q_b (NU) correspondingly, prior to and following adsorption on the nanosheets. According to the Hirshfeld charge analysis, during the interaction of NU on these four nanosheets, an amount of charge of about 0.08, 0.25, 0.03, 0.03 e and 0.36, 0.39, 0.11, 0.08 e was transferred to the AlN, AlN/GaN (H1), GaN and GaN/AlN (H2) in state 1 from NU drug in air media and water media, respectively.

In state 2, about 0.13, −0.03, 0.07, −0.05 e and 0.21, −0.04, 0.12, −0.13 e was transferred to the AlN, AlN/GaN (H1), GaN and GaN/AlN (H2) from NU drug in air media and water media,

(a) AlN

(b) AlN/GaN (H1)

(c) GaN

(d) GaN/AlN (H2)

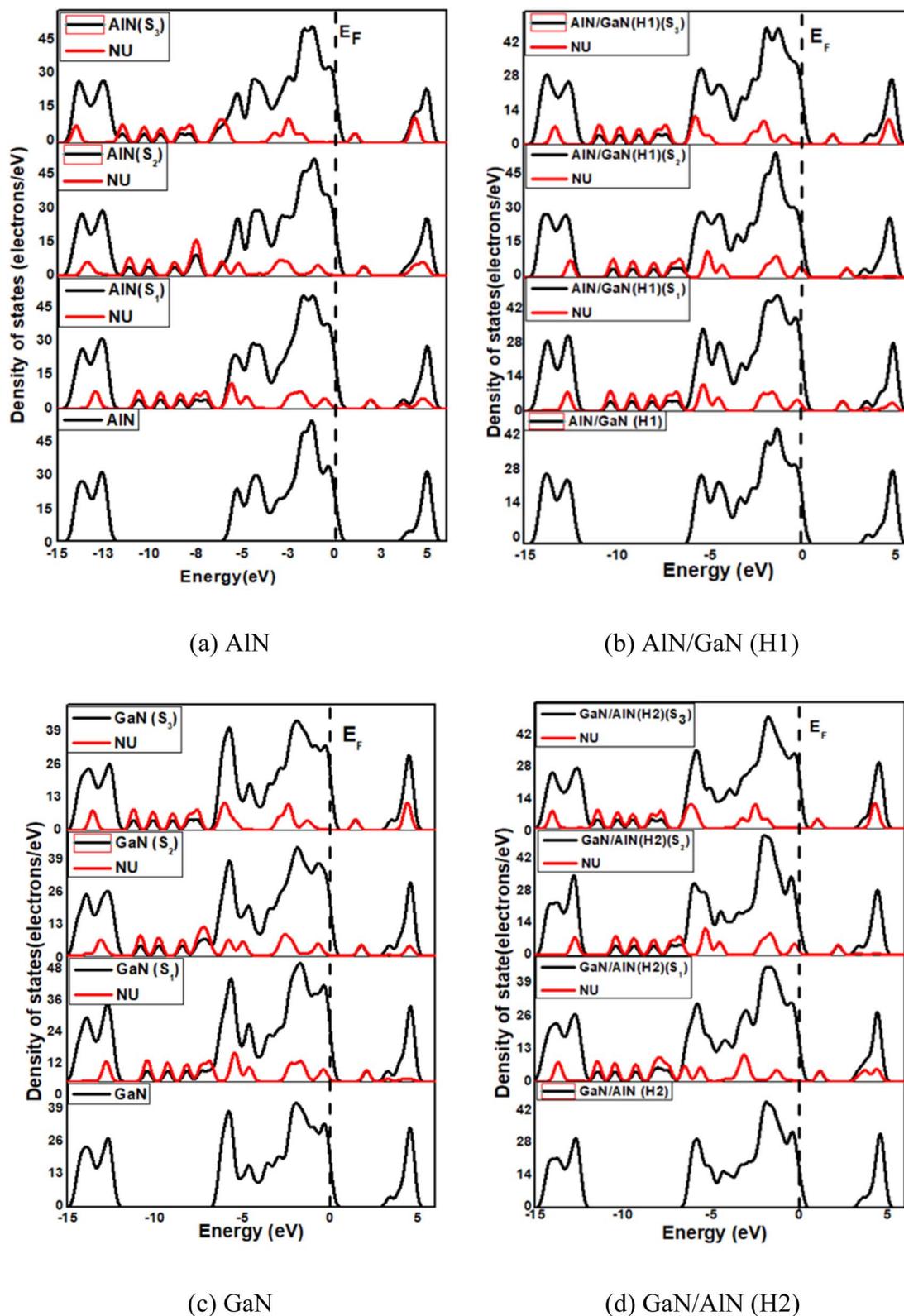Fig. 2 (a)–(d) DOS and PDOS spectra of the pristine and their in-plane heterostructures nanosheets before and after adsorption of NU drug.
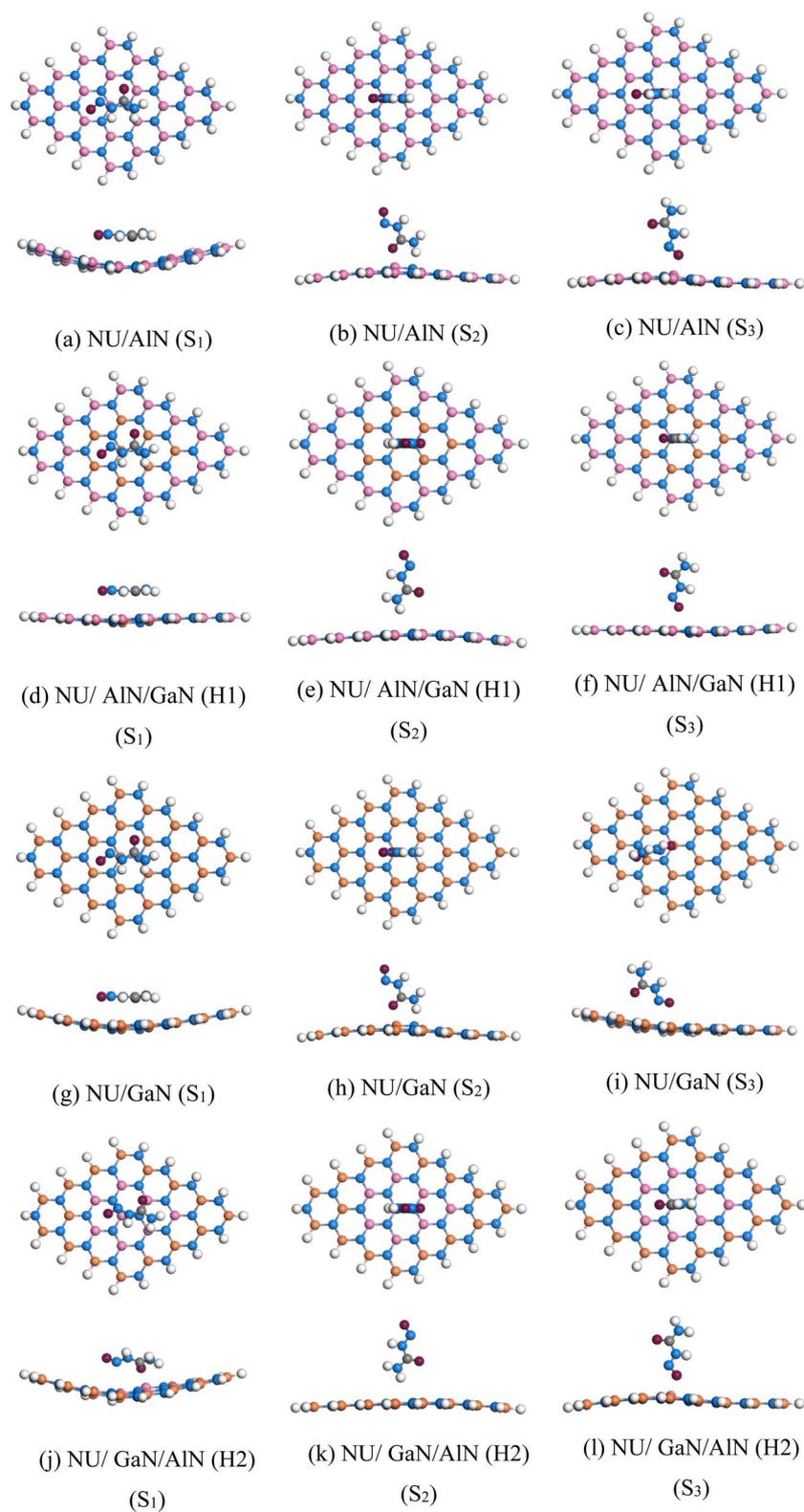
(a) NU/AlN (S$_1$)

(b) NU/AlN (S$_2$)

(c) NU/AlN (S$_3$)

(d) NU/ AlN/GaN (H1) (S$_1$)

(e) NU/ AlN/GaN (H1) (S$_2$)

(f) NU/ AlN/GaN (H1) (S$_3$)

(g) NU/GaN (S$_1$)

(h) NU/GaN (S$_2$)

(i) NU/GaN (S$_3$)

(j) NU/ GaN/AlN (H2) (S$_1$)

(k) NU/ GaN/AlN (H2) (S$_2$)

(l) NU/ GaN/AlN (H2) (S$_3$)

Fig. 3 (a)–(l) Top and side views of the stable optimized complexes.

Table 1 Calculated adsorption energy E_{Ad} in (eV), minimum interaction distance d in (Å), charge transfer Q_{HS} in (e) in air and water media

Structures	States	Air media			Water media		
		E_{Ad}	Q_{HS}	d	E_{Ad}	Q_{HS}	d
NU/AlN	S1	−0.59	0.08	3.11	−0.67	0.36	3.00
	S2	−0.94	0.13	1.77	−0.75	0.21	1.89
	S3	−0.46	0.21	2.11	−0.54	0.36	2.06
NU/AlN/GaN (H1)	S1	−0.74	0.25	2.06	−0.76	0.39	1.98
	S2	−0.18	−0.03	2.79	−0.05	−0.04	2.72
	S3	−0.41	0.21	2.12	−0.56	0.34	2.06
NU/GaN	S1	−0.63	0.03	3.09	−0.39	0.11	3.06
	S2	−0.72	0.07	1.85	−0.51	0.12	1.87
	S3	−0.43	0.16	2.64	−0.37	0.32	2.33
NU/GaN/AlN (H2)	S1	−0.64	0.03	3.14	−0.36	0.08	3.27
	S2	−0.24	−0.05	2.71	−0.19	−0.13	2.02
	S3	−0.23	0.12	2.59	−0.22	0.21	2.32

respectively. In state 3, about 0.21, 0.21, 0.16, 0.12 e and 0.36, 0.34, 0.32, 0.21 e was transferred to the AlN, AlN/GaN (H1), GaN and GaN/AlN (H2) from NU drug in air media and water media, respectively.

Frontier molecular orbital (FMO) as well as energy gap (E_g) analyses were performed and the results are tabulated in Table 2. Fig. 4 shows the FMO maps of the stable complexes of the NU/nanosheets. The HOMO levels were located at −5.54, −5.43, −5.47 and −5.57 eV and −5.44, −56, −5.62 and −5.48 eV in air and water media, LUMO levels at −1.69, −1.89, −2.09 and −2.03 eV and −1.61, −1.96, −2.21 and −1.98 eV in air and water media for AlN, AlN/GaN (H1), GaN and GaN/AlN (H2) nanosheets.

After adsorption of NU on the nanosheets, the HOMO and LUMO levels varied. For example, for AlN, AlN/GaN (H1), GaN and GaN/AlN (H2), the HOMO levels were change from −5.43 and −5.57 to −5.27 and −5.65 eV while the LUMO levels increased from −1.89 and −2.03 eV to −4.13 and −3.46 eV, respectively. The HOMO and LUMO gap, *i.e.*, the energy gap,

was also calculated and it was found that the energy gap was reduced from 3.54 to 1.15 eV and 3.54 to 3.46 eV for AlN/GaN (H1) and AlN/GaN (H2) nanosheets. The conductivity (σ) of these nanosheets was exponentially enhanced due to the reduction in the energy gap and maintained the following relation,[44]

$$\sigma \propto e^{\left(\frac{-E_g}{2kT}\right)} \quad (9)$$

where, k is Boltzmann's constant = 1.380×10^{-23} m² kg⁻² k⁻¹. The NU drug was adsorbed in the center of the nanosheets in a parallel arrangement in order to study the adsorption phenomena of NU on the AlN, AlN/GaN (H1), GaN and GaN/AlN (H2). Prior research indicated that when drug molecules were arranged parallel to the nanosheets, they were favorably adsorbed on them.[47]

3.3 Dipole moment

Another crucial analysis that shows the asymmetric charge distribution in a complex is the dipole moment (DM). The asymmetric charge distribution and reactivity of a system can also be explained by the dipole moment, as is widely known. A molecule is considered nonpolar when its dipole moment is zero.[41]

In Table 3, the dipole moments of the various nanosheets and complexes are recorded. In polar solvents, greater reactivity and solubility are indicated by a high dipole moment value. Following the NU drug adsorption on the nanosheets, the dipole moment value rise, suggesting that the drug can flow freely across biological systems. The dipole moments of our pristine AlN, AlN/GaN (H1), GaN and GaN/AlN (H2) nanosheets were 4.52, 2.86, 2.72 and 4.62 D and 6.57, 3.69, 3.47 and 6.82 D before the adsorption process in air media and water media, respectively. After NU interacted with the nanosheets, the dipole moments rise, specifically to 8.33, 6.95, 6.31 and 8.18 D and

Table 2 HOMO energy (E_{HOMO}), LUMO energy (E_{LUMO}), HOMO–LUMO energy gap (E_g) in eV, change in energy gap ($\%E_g$) in air and water media

Structures	States	Air media				Water media			
		E_{HOMO}	E_{LUMO}	E_g	$\%E_g$	E_{HOMO}	E_{LUMO}	E_g	$\%E_g$
AlN		−5.54	−1.69	3.84	0	−5.44	−1.61	3.83	0
NU/AlN	S1	−5.59	−3.73	1.87	−51.33	−5.23	−3.73	1.51	−60.65
	S2	−5.51	−4.01	1.49	−61.01	−5.38	−3.59	1.79	46.88
	S3	−5.39	−4.37	1.01	−73.63	−5.33	−3.83	1.49	−60.99
AlN/GaN (H1)		−5.43	−1.89	3.54	0	−5.56	−1.96	3.61	0
NU/AlN/GaN (H1)	S1	−5.27	−4.13	1.15	−67.62	−5.41	−3.91	1.51	−58.11
	S2	−5.43	−3.23	2.19	−37.92	−5.58	−3.45	2.13	−40.87
	S3	−5.31	−4.29	1.02	−71.09	−5.48	−3.98	1.49	−58.63
GaN		−5.47	−2.09	3.37	0	−5.62	−2.21	3.41	0
NU/GaN	S1	−5.51	−3.44	2.07	−38.67	−5.62	−3.61	2.02	−40.86
	S2	−5.44	−3.67	1.77	−47.39	−5.59	−3.66	1.94	−43.21
	S3	−5.31	−3.86	1.44	−57.18	−5.57	−3.81	1.76	−48.43
GaN/AlN (H2)		−5.57	−2.03	3.54	0	−5.49	−1.98	3.51	0
NU/GaN/AlN (H2)	S1	−5.65	−3.46	2.18	−38.23	−5.48	−3.41	2.07	−40.84
	S2	−5.59	−3.17	2.42	−31.71	−5.51	−3.26	2.25	−35.82
	S3	−5.47	−3.83	1.64	−53.61	−5.45	−3.68	1.78	−49.23

HOMO	LUMO	HOMO	LUMO

(a) NU/AlN (S$_1$)   (b) NU/AlN (S$_2$)

(c) NU/AlN (S$_3$)   (d) NU/ AlN/GaN (H1) (S$_1$)

(e) NU/ AlN/GaN (H1) (S$_2$)   (f) NU/ AlN/GaN (H1) (S$_3$)

(g) NU/GaN (S$_1$)   (h) NU/GaN (S$_2$)

(i) NU/GaN (S$_3$)   (j) NU/ GaN/AlN (H2) (S$_1$)

(k) NU/ GaN/AlN (H2) (S$_2$)   (l) NU/ GaN/AlN (H2) (S$_3$)
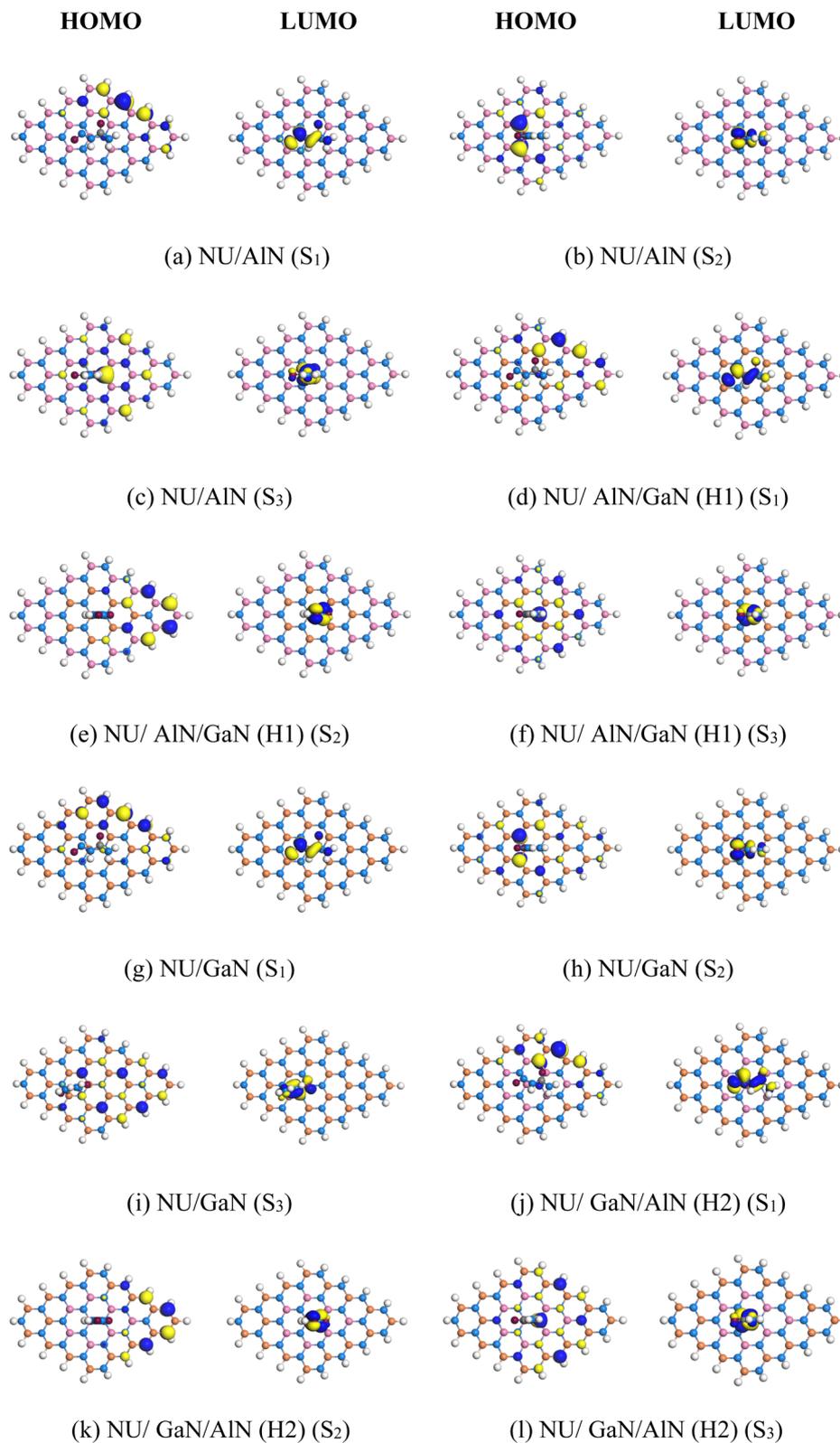
Fig. 4 (a)–(l) HOMO and LUMO maps of the stable complexes.

Table 3 Dipole moment (D.M) in Debye and solvation energy (E_{solv}) in eV for the nanosheets and complexes in air and water media

Structures	States	D. M (air)	D. M (water)	E_{solv} (eV)
AlN		4.52	6.57	−0.61
NU/AlN	S1	8.33	16.08	−1.39
	S2	10.01	15.57	−1.12
	S3	11.06	15.56	−1.39
AlN/GaN (H1)		2.86	3.69	−0.73
NU/AlN/GaN (H1)	S1	6.95	13.96	−1.46
	S2	4.09	7.28	−1.31
	S3	9.68	14.62	−1.58
GaN		2.72	3.47	−0.89
NU/GaN	S1	6.31	11.33	−1.36
	S2	7.67	12.07	−1.39
	S3	7.94	13.56	−1.55
GaN/AlN (H2)		4.62	6.82	−0.68
NU/GaN/AlN (H2)	S1	8.18	13.13	−1.09
	S2	3.98	8.38	−1.35
	S3	10.09	16.71	−1.38

16.08, 13.96, 11.33 and 13.13 D in air media and water media, respectively.

The solubility of the nanosheets in polar media was enhanced due to the increased dipole moments mentioned above. The most reactive of these complexes were NU/AlN, NU/AlN/GaN (H1), NU/GaN and NU/GaN/AlN (H2), based on the charge-transfer and dipole moment analyses. Because of their high dipole moment in the media, these four complexes also shown increased reactivity in water solvent media. Following the adsorption of NU drug, the dipole moment of the four nanosheets was amplified by approximately two to three times in the dipole. In Fig. 5, a bar diagram that compares the dipole moments in water and air media was displayed.
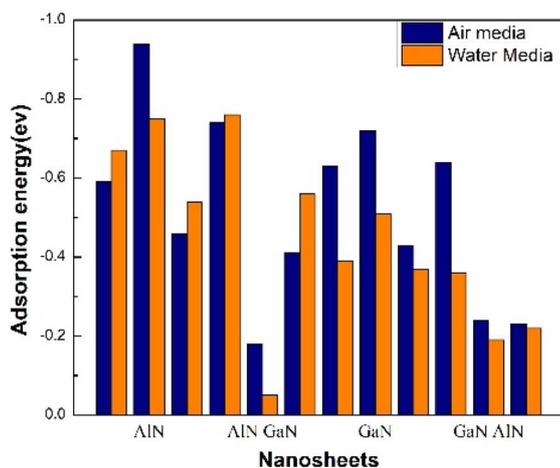
3.4 Desorption time

Another essential component of a drug delivery system is the desorption time which significantly influence the drug-release mechanism. In this instance, we used the van't Hoff-Arrhenius and transition-state theories to determine the drug desorption periods from the nanosheets as follows:

$$\tau = \frac{1}{\vartheta_0} \exp\left(\frac{-E_{ads}}{k_B T}\right) \tag{10}$$

The desorption time was determined by taking into account three different temperatures: room temperature (298 K), normal body temperature (310 K) and cancer tissue temperature (315 K); the attempt frequency (10^{12} Hz) was denoted by ϑ_o and Boltzmann's constant was represented by k_B. At cancer tissue temperature, the desorption time was 0.002, 0.75, 0.011 and 0.021 s in air media and 0.062, 1.73, 1.75×10^{-6} and 5.27×10^{-7} s in water media. This duration was exponentially dependent on the adsorption of NU on the AlN, AlN/GaN (H1), GaN and GaN/AlN (H2) nanosheets (Table 4).

3.5 Quantum molecular descriptors

Quantum molecular descriptors, such as the chemical potential (μ), global hardness (η), global softness (S) and electrophilicity index (ω) have been investigated to predict the reactivity of the nanosheets toward NU drug.[45] The chemical potential indicates the tendency for an electron to escape from an equilibrium position. The calculated values of the chemical potentials of the nanosheets were enhanced after the adsorption of NU drug. The calculated chemical potentials for the AlN, AlN/GaN (H1), GaN and GaN/AlN (H2) nanosheets were 3.62, 3.66, 3.78 and 3.81 eV, respectively. After adsorption of NU on the nanosheets, the values were enhanced to 4.66, 4.69, 4.47 and 4.56 eV, respectively. The reactivity of complexes is also defined by two other

(a)
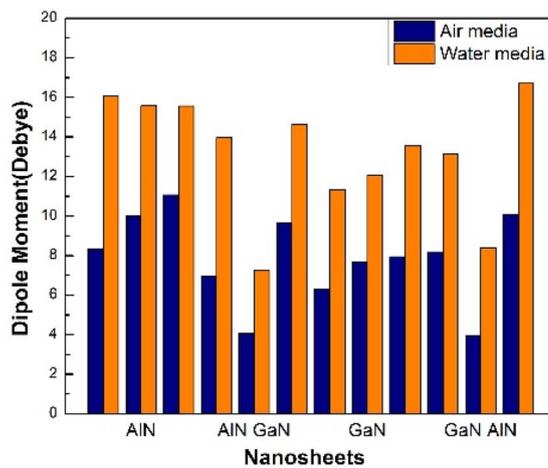
(b)

Fig. 5 Comparison of the (a) adsorption energy and (b) dipole moment in the air and water media.

Table 4 NU drug desorption time at room temperature (298 K), body temperature (310 K) and cancer tissue temperature (315 K) in air and water media

Structures	States	Air media			Water media		
		298 K	310 K	315 K	298 K	310 K	315 K
NU/AlN	S1	0.009	0.003	0.002	0.256	0.093	0.062
	S2	9389.39	2261.22	1290.09	5.319	1.711	1.094
	S3	5.38×10^{-5}	2.69×10^{-5}	2.06×10^{-5}	0.001	0.0005	0.0003
NU/AlN/GaN (H1)	S1	3.59	1.17	0.75	8.62	2.72	1.73
	S2	1.01×10^{-9}	7.73×10^{-10}	6.95×10^{-10}	7.16×10^{-12}	6.64×10^{-12}	6.44×10^{-12}
	S3	9.11×10^{-6}	4.89×10^{-6}	3.84×10^{-6}	0.003	0.001	0.0008
NU/GaN	S1	0.04	0.02	0.011	3.97×10^{-6}	2.21×10^{-6}	1.75×10^{-6}
	S2	1.32	0.45	0.29	0.0004	0.001	0.0001
	S3	1.54×10^{-5}	8.09×10^{-6}	6.29×10^{-6}	2.22×10^{-6}	1.26×10^{-6}	1.01×10^{-6}
NU/GaN/AlN (H2)	S1	0.08	0.03	0.021	1.12×10^{-6}	6.52×10^{-7}	5.27×10^{-7}
	S2	9.47×10^{-9}	6.64×10^{-9}	5.78×10^{-9}	2.35×10^{-9}	1.74×10^{-9}	1.59×10^{-9}
	S3	6.32×10^{-9}	4.51×10^{-9}	3.94×10^{-9}	5.01×10^{-9}	3.59×10^{-9}	3.16×10^{-9}

crucial parameters: global hardness and softness.[46] When an external electric field is present, a structures resistance to deformation reveals its global hardness values. Higher global hardness values signify that the nanosheets are more robust when exposed to an electric field. Global softness and global hardness are inversely related. A greater reactivity of the nanosheets is implied by higher global softness values. The global hardness and global softness values in the air and water medium decreased and increased in Table 5 confirming that all of the nanosheets demonstrated reactivity following the adsorption of the NU drug. The electrophilicity index was also computed to examine the nanosheets electrophilic power or their capacity to take up electrons. According to our computed values, all of the nanosheets exhibited strong electrophilicity following interaction with the NU drug. The AlN, AlN/GaN (H1), GaN and GaN/AlN (H2) nanosheets have the potential to be used as drug carriers for NU in water media, as evidenced by the greater dipole moment values of the nanosheets in the water media as opposed to the air media.

3.6 Solvent effect

To investigate the solvent effect on the complexes, the solvation energy, adsorption energy, electronic properties and dipole moment in water media were calculated and showed in Tables 2 and 4 The difference between the complexes total energy in the water and air media was used to compute the solvation energy as indicated below,[47]

$$E_{solv} = E_{water} - E_{air} \tag{11}$$

where, E_{air} and E_{water} are the energy of air and water media. In the water media, the complexes stability and solubility were demonstrated by their negative solvation energy values. Our solvation energy calculations revealed that all four of the nanosheets were stable in water medium. The nanosheets great stability in the water media was suggested by the solvation energies becoming more negative following the NU adsorption on them. The calculated values were −0.59, −0.74, −0.63 and −0.64 eV for the AlN, AlN/GaN (H1), GaN and GaN/AlN (H2)

Table 5 Values of the chemical potential (μ), global hardness (η), electrophilicity index (ω) in unit eV, nucleophilicity index (ν) and global softness (S) in unit eV^{-1} in air and water media

Structures	States	Air media					Water media				
		μ (eV)	η (eV)	S (eV^{-1})	ω (eV)	ϑ (eV^{-1})	μ (eV)	η (eV)	S (eV^{-1})	ω (eV)	ϑ (eV^{-1})
AlN		3.62	1.92	0.26	3.41	0.29	3.52	1.92	0.26	3.24	0.31
NU/AlN	S1	4.66	0.94	0.54	11.63	0.09	4.48	0.75	0.66	13.32	0.08
	S2	4.76	0.75	0.67	15.09	0.07	4.49	0.89	0.56	11.22	0.09
	S3	4.88	0.51	0.99	23.51	0.04	4.58	0.75	0.67	14.05	0.07
AlN/GaN (H1)		3.66	1.77	0.28	3.79	0.26	3.76	1.81	0.28	3.93	0.25
NU/AlN/GaN (H1)	S1	4.69	0.57	0.87	19.27	0.05	4.66	0.76	0.66	14.38	0.07
	S2	4.33	1.09	0.46	8.54	0.12	4.52	1.07	0.47	9.58	0.11
	S3	4.81	0.51	0.97	22.53	0.04	4.73	0.75	0.67	15.02	0.07
GaN		3.78	1.69	0.29	4.24	0.24	3.92	1.71	0.29	4.51	0.22
NU/GaN	S1	4.47	1.03	0.48	9.68	0.11	4.61	1.01	0.49	10.53	0.09
	S2	4.55	0.89	0.56	11.69	0.08	4.63	0.97	0.52	11.06	0.09
	S3	4.58	0.72	0.69	14.53	0.07	4.69	0.88	0.57	12.52	0.08
GaN/AlN (H2)		3.81	1.77	0.28	4.09	0.25	3.73	1.75	0.29	3.98	0.25
NU/GaN/AlN (H2)	S1	4.56	1.09	0.46	9.49	0.11	4.45	1.04	0.48	9.55	0.12
	S2	4.38	1.21	0.41	7.95	0.13	4.38	1.13	0.45	8.53	0.13
	S3	4.65	0.82	0.61	13.19	0.09	4.56	0.89	0.56	11.67	0.08

Table 6 Fermi level energies (E_F) in eV, work function (ϕ) in eV and change in work function (% ϕ) for the nanosheets and complexes in air and water media

Structures	States	Air media			Water media		
		E_F	ϕ	% $\Delta\phi$	E_F	ϕ	% $\Delta\phi$
AlN		−0.131	0.131	0	−0.127	0.127	0
NU/AlN	S1	−0.169	0.169	29.32	−0.162	0.162	27.59
	S2	−0.172	0.172	31.77	−0.163	0.163	27.53
	S3	−0.176	0.176	34.89	−0.165	0.165	29.98
AlN/GaN (H1)		−0.132	0.132	0	−0.136	0.136	0
NU/AlN/GaN (H1)	S1	−0.171	0.171	29.15	−0.171	0.171	25.71
	S2	−0.157	0.157	18.86	−0.157	0.157	15.69
	S3	−0.173	0.173	31.17	−0.173	0.173	27.67
GaN		−0.136	0.136	0	−0.141	0.141	0
NU/GaN	S1	−0.161	0.162	18.67	−0.166	0.166	17.83
	S2	−0.164	0.164	20.63	−0.167	0.167	18.21
	S3	−0.165	0.165	21.12	−0.169	0.169	19.67
GaN/AlN (H2)		−0.137	0.137	0	−0.135	0.135	0
NU/GaN/AlN (H2)	S1	−0.164	0.164	19.83	−0.161	0.161	19.37
	S2	−0.158	0.158	15.44	−0.158	0.158	17.74
	S3	−0.168	0.168	22.45	−0.164	0.164	22.12

nanosheets after the interaction of NU with these nanosheets, the solvation energies were enhanced to −1.39, −1.46, −1.36 and −1.09 eV, respectively. The adsorption energies in the water media were also calculated and confirm the attractive interaction between the NU and nanosheets due to their negative adsorption energies. The calculated values of the adsorption energies were −0.59, −0.74, −0.63 and −0.64 eV for the AlN, AlN/GaN (H1), GaN and GaN/AlN (H2) nanosheets, respectively. During the interaction, the NU drug transfers −0.01, −0.05, −0.03, and −0.02 e to the nanosheets, respectively. The drug was adsorbed by keeping 3.11, 2.06, 3.09 and 3.14 Å distance from the nanosheets.

3.7 Work function

The least amount of energy needed to extract a single electron from the Fermi level is known as the work function. The purpose of this study is to determine if the NU impacts the work function of the nanosheets and it is computed using the following equation:[48]

$$\phi = V_{el}(+\infty) - E_F \tag{12}$$

where, E_F, ϕ and $V_{el}(+\infty)$ denote the Fermi level energy, work function and electrostatic potential of an electron far away from the surface, respectively. However, $V_{el}(+\infty)$ is considered to be zero. Eqn (12) may be expressed as $\phi = -E_F$. The calculated values of Fermi level (E_F), work function (ϕ) and change in work function ($\Delta\phi$) are tabulated in Table 6.

Now, the following formula is used to calculate the change in work function after adsorption,[49]

$$\phi = \frac{\phi_f - \phi_i}{\phi_i} \times 100\% \tag{13}$$

where, ϕ_i and ϕ_f denote the work functions before and after adsorption, respectively. A change in ϕ alters the gate voltage, induces an electrical signal and is a useful indicator for

chemical sensing applications.[50] The intrinsic work function values of were found to be −0.131, −0.132, −0.136, and −0.137 eV in AlN, AlN/GaN (H1), GaN and GaN/AlN (H2) in air media, respectively. And work function values of were found to be −0.27, −0.136, −0.141, and −0.135 eV in AlN, AlN/GaN (H1), GaN and GaN/AlN (H2) in water media, respectively. After NU adsorption, noticeable changes in the work function were observed. AlN, AlN/GaN (H1), GaN and GaN/AlN (H2) in air media for state 1 work function values of −0.169, −0.157, −0.161 and −0.164 eV. For the AlN nanosheet, ϕ increased slightly in all configurations, with the highest change being 2.58% in S_3. GaN/AlN (H2) showed substantial increases, with a maximum change of 25.21% in S_3. The AlN/GaN (H1) nanosheet exhibited the most significant work function variation, reaching up to 28.36% in S_1. For GaN, the change was also notable, with values ranging from 17.83% to 19.67%.

3.8 COSMO surface analysis

To gain more insights into the solvent effect, COSMO surface analysis of our complexes was performed. The visualization of the COSMO surfaces, as shown in Fig. 6, illustrates the polar and non-polar regions of the complexes. A positively charged region known as a hydrogen bond donor (HBD) is indicated by the red section of this COSMO surface. On the other hand, the complexes negatively charged hydrogen bond acceptor (HBA) region is shown by the blue section. Additionally, a neutral and non-polar section of the complexes are implied by the yellowish green part. In our study, it was evident that the HBD region grew after the NU was adsorbed on the nanosheets, particularly on the AlN, AlN/GaN (H1), GaN and GaN/AlN (H2) nanosheets. This suggested that the complexes were highly polar in the water solvent medium. The impact of complexes on solvation by calculating the dipole moment, electrical properties, and adsorption energy in the water media. In this work, conductor-like screening model (COSMO) surface analysis was carried out to provide an understanding of the biological environment
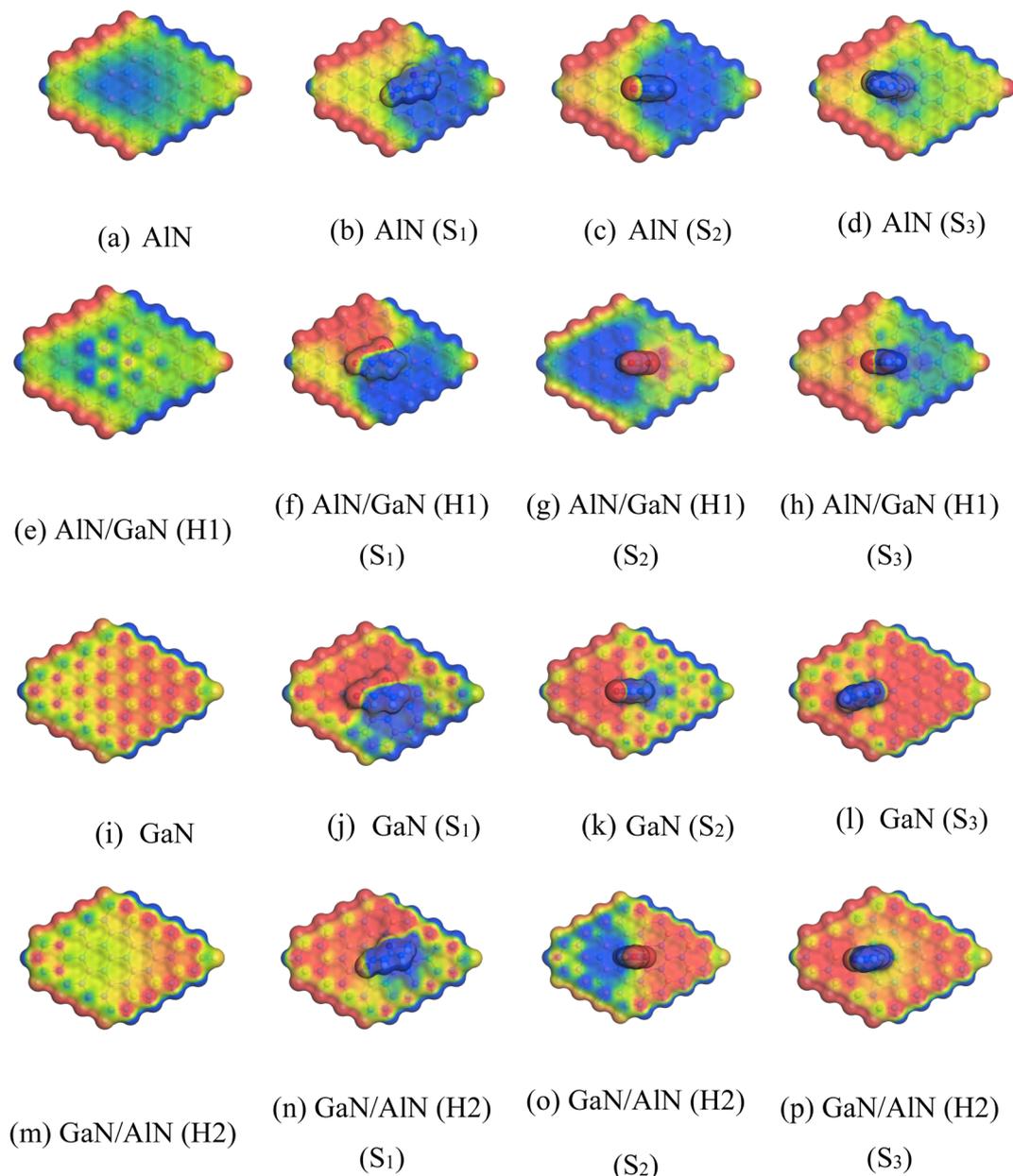
Fig. 6 (a)−(p) Front views of the COSMO surfaces of the before and after adsorption of NU.

4. Conclusions

Recently, a lot of research has been done on using nano-materials to lessen the immediate adverse effects of chemo-therapy in the treatment of cancer. Using the DFT approach, the surface adsorption of NU on AlN, AlN/GaN (H1), GaN and GaN/AlN (H2) nanosheets was examined in air and water media. To understand the adsorption behavior of NU on the nanosheets, the adsorption energies and distances, charge transfer, electronic characteristics (HOMO, LUMO, and E_g), solvation

energies, as well as QMD and COSMO surface were examined. According to our calculations, the NU adsorbed on these four nanosheets (AlN, AlN/GaN (H1), GaN and GaN/AlN (H2)) with adsorption energies of −0.94, −0.74, −0.72, −0.64 eV and −0.75, −0.76, −0.51, −0.36 eV by transferring 0.13, 0.25, 0.07, 0.03 e and 0.21, 0.39, 0.12, 0.08 e charges to the nanosheets in both air and water media, respectively. The structures relative energy gaps were determined to be 3.84, 3.54, 3.37 and 3.54 eV. Following the adsorption of NU on the nanosheets, discernible peaks emerged in the Fermi level from the DOS spectra, indicating the closing of the energy gap. The NU drug significantly increases the electrical conductivity which can be transformed into an electrical signal by lowering the nanosheets E_g. Dipole moment and COSMO analyses also proved that the four

nanosheets showed high asymmetry and solubility in water media. The calculated dipole moments of the AlN, AlN/GaN (H1), GaN and GaN/AlN (H2) nanosheets in air media were 4.52, 2.86, 2.72 and 4.62 D and in water media were 6.57, 3.69, 3.47 and 6.82 D. But after interaction with NU drug, the dipole moments increased to 8.33, 6.95, 6.31 and 8.18 D in air media and 16.08, 13.96, 11.33 and 13.13 D in water media, respectively. Moreover, the quantum molecular descriptors indicated that the nanosheets reactivity and sensitivity were improved during the interaction with NU. According to our research, AlN and GaN based nanomaterials showed great promise as effective and selective NU carriers. Among them AlN in state 2 showed best reactivity as NU drug carrier.

Conflicts of interest

The authors have declared no conflict of interest.

Data availability

All data supporting the findings of this study, including optimized structures, adsorption energy values, charge transfer, work function, *etc.*, are available within the article. All the calculations have been implemented by the DMol^3 module in BIOVIA Materials Studio 2017. Additional data can be provided by the corresponding author upon reasonable request.

Acknowledgements

References

1 G. R. Sarria, D. A. Martinez, R. Del Castillo, *et al.*, Radiotherapy and cancer status in Latin America: economic analysis of investment opportunities up to 2030, *Lancet Oncol.*, 2022, **23**(1), S5, DOI: 10.1016/s1470-2045(22)00404-1.

2 A. A. Piya and A. K. M. A. Hossain, Investigation of the adsorption behavior of the anti-cancer drug hydroxyurea on the graphene, BN, AlN, and GaN nanosheets and their doped structures *via* DFT and COSMO calculations, *RSC Adv.*, 2023, **13**(39), 27309–27320, DOI: 10.1039/d3ra04072k.

3 Y. Fukuyo, C. R. Hunt and N. Horikoshi, Geldanamycin and its anti-cancer activities, *Cancer Lett.*, 2010, **290**(1), 24–35, DOI: 10.1016/j.canlet.2009.07.010.

4 K. A. Hoadley, C. Yau, T. Hinoue, *et al.*, Cell-of-Origin Patterns Dominate the Molecular Classification of 10 000 Tumors from 33 Types of Cancer, *Cell*, 2018, **173**(2), 291–304, DOI: 10.1016/j.cell.2018.03.022.

5 National Cancer Institute, *Common Cancer Types*, published online 2024.

6 Z. Abbas and S. Rehman, An Overview of Cancer Treatment Modalities, *Neoplasm*, 2018, **1**, 139–157, DOI: 10.5772/intechopen.76558.

7 J. J. Wang, K. F. Lei and F. Han, Tumor microenvironment: recent advances in various cancer treatments, *Rev. Eur. Sci. Med. Pharmacol.*, 2018, **22**(12), 3855–3864, DOI: 10.26355/eurrev-201806-15270.

8 P. Nygren, What is cancer chemotherapy?, *Acta Oncol.*, 2001, **40**(2–3), 166–174, DOI: 10.1080/02841860151116204.

9 J. Gao, Y. Liang and L. Wang, Shaping Polarization Of Tumor-Associated Macrophages In Cancer Immunotherapy, *Front. Immunol.*, 2022, **13**, 888713, DOI: 10.3389/fimmu.2022.888713.

10 L. L. Bu, J. Yan, Z. Wang, *et al.*, Advances in drug delivery for post-surgical cancer treatment, *Biomaterials*, 2019, **219**, 119182, DOI: 10.1016/j.biomaterials.2019.04.027.

11 S. Nussbaumer, P. Bonnabry, J. L. Veuthey and S. Fleury-Souverain, Analysis of anticancer drugs: a review, *Talanta*, 2011, **85**(5), 2265–2289, DOI: 10.1016/j.talanta.2011.08.034.

12 R. Rahimi and M. Solimannejad, BC3 graphene-like monolayer as a drug delivery system for nitrosourea anticancer drug: a first-principles perception, *Appl. Surf. Sci.*, 2020, **525**, 146577, DOI: 10.1016/j.apsusc.2020.146577.

13 H. Y. P. Lam, A. Begleiter, G. J. Goldenberg and C. M. Wong, Synthesis of Steroidal Nitrosoureas with Antitumor Activity, *J. Med. Chem.*, 1979, **22**(2), 200–202, DOI: 10.1021/jm00188a015.

14 M. Rosten, Hydroxyurea: A New Antimetabolite In The Treatment Of Psoriasis, *Br. J. Dermatol.*, 1971, **85**(2), 177–181, DOI: 10.1111/j.1365-2133.1971.tb07206.x.

15 A. I. Schafer, Management of thrombocythemia, *Curr. Opin. Hematol.*, 1996, **3**(5), 341–346, DOI: 10.1097/00062752-199603050-00002.

16 C. A. Sabin and J. D. Lundgren, The natural history of HIV infection, *Curr. Opin. HIV AIDS*, 2013, **8**(4), 311–317, DOI: 10.1097/COH.0b013e328361fa66.

17 T. L. Murphy and K. M. Murphy, Dendritic cells in cancer immunology, *Cell. Mol. Immunol.*, 2022, **19**(1), 3–13, DOI: 10.1038/s41423-021-00741-5.

18 A. N. Schechter and G. P. Rodgers, Sickle Cell Anemia — Basic Research Reaches the Clinic, *N. Engl. J. Med.*, 1995, **332**(20), 1372–1374, DOI: 10.1056/nejm199505183322010.

19 S. Charache, G. J. Dover, M. A. Moyer and J. W. Moore, Hydroxyurea-induced augmentation of fetal hemoglobin production in patients with sickle cell anemia, *Blood*, 1987, **69**(1), 109–116, DOI: 10.1182/blood.v69.1.109.bloodjournal691109.

20 N. Sushma, K. Jessica Vevina and H. Shoeb, A Study On Nanotechnology For Cancer Treatment, *YMER Digit*, 2022, **21**(05), 669–680, DOI: 10.37896/ymer21.05/77.

21 R. Misra, S. Acharya and S. K. Sahoo, Cancer nanotechnology: application of nanotechnology in cancer therapy, *Drug Discovery Today*, 2010, **15**(19–20), 842–850, DOI: 10.1016/j.drudis.2010.08.006.

22 M. Arif, A. F. Nawaz, S. Ullah khan, *et al.*, Nanotechnology-based radiation therapy to cure cancer and the challenges in its clinical applications, *Heliyon*, 2023, **9**(6), e17252, DOI: 10.1016/j.heliyon.2023.e17252.

23 P. Zhang, T. Han, H. Xia, L. Dong, L. Chen and L. Lei, Advances in Photodynamic Therapy Based on Nanotechnology and Its Application in Skin Cancer, *Front. Oncol.*, 2022, **12**, 836397, DOI: 10.3389/fonc.2022.836397.

24 M. S. Aslam, S. Naveed, A. Ahmed, Z. Abbas, I. Gull and M. A. Athar, Side Effects of Chemotherapy in Cancer Patients and Evaluation of Patients Opinion about Starvation Based Differential Chemotherapy, *J. Cancer Ther.*, 2014, **05**(08), 817–822, DOI: 10.4236/jct.2014.58089.

25 A. N. Banerjee, Graphene and its derivatives as biomedical materials: future prospects and challenges, *Interface Focus*, 2018, **8**(3), 20170056, DOI: 10.1098/rsfs.2017.0056.

26 A. Vaidyanathan, M. Mathew, S. Radhakrishnan, C. S. Rout and B. Chakraborty, Theoretical Insight on the Biosensing Applications of 2D Materials, *J. Phys. Chem. B*, 2020, **124**(49), 11098–11122, DOI: 10.1021/acs.jpcb.0c08539.

27 A. Li, J. Yang, Y. He, J. Wen and X. Jiang, Advancing piezoelectric 2D nanomaterials for applications in drug delivery systems and therapeutic approaches, *Nanoscale Horiz.*, 2024, **9**(3), 365–383, DOI: 10.1039/d3nh00578j.

28 M. Ayoubi-Chianeh and M. Z. Kassaee, Detection of bendamustine anti-cancer drug *via* AlN and Si-doped C nanocone and nanosheet sensors by DFT, *Struct. Chem.*, 2020, **31**(5), 2041–2050, DOI: 10.1007/s11224-020-01561-5.

29 H. L. Guo, X. F. Wang, Q. Y. Qian, F. B. Wang and X. H. Xia, A green approach to the synthesis of graphene nanosheets, *ACS Nano*, 2009, **3**(9), 2653–2659, DOI: 10.1021/nn900227d.

30 H. O. Edet, H. Louis, T. E. Gber, *et al.*, Heteroatoms (B, N, S) doped quantum dots as potential drug delivery system for isoniazid: insight from DFT, NCI, and QTAIM, *Heliyon*, 2023, **9**(1), e12599, DOI: 10.1016/j.heliyon.2022.e12599.

31 B. Delley, An all-electron numerical method for solving the local density functional for polyatomic molecules, *J. Chem. Phys.*, 1990, **92**(1), 508–517, DOI: 10.1063/1.458452.

32 B. Delley, From molecules to solids with the DMol3 approach, *J. Chem. Phys.*, 2000, **113**(18), 7756–7764, DOI: 10.1063/1.1316015.

33 J. P. Perdew, K. Burke and M. Ernzerhof, Generalized gradient approximation made simple, *Phys. Rev. Lett.*, 1996, **77**(18), 3865, DOI: 10.1103/PhysRevLett.77.3865.

34 J. P. Perdew and A. Zunger, Self-interaction correction to density-functional approximations for many-electron systems, *Phys. Rev. B:Condens. Matter Mater. Phys.*, 1981, **23**(10), 5048, DOI: 10.1103/PhysRevB.23.5048.

35 S. Grimme, Semiempirical GGA-type density functional constructed with a long-range dispersion correction, *J. Comput. Chem.*, 2006, **27**(15), 1787–1799, DOI: 10.1002/jcc.20495.

36 B. Delley, Hardness conserving semilocal pseudopotentials, *Phys. Rev. B:Condens. Matter Mater. Phys.*, 2002, **66**(15), 155125, DOI: 10.1103/PhysRevB.66.155125.

37 H. P. Zhang, X. G. Luo, H. T. Song, X. Y. Lin, X. Lu and Y. Tang, DFT study of adsorption and dissociation behavior of H 2 S on Fe-doped graphene, *Appl. Surf. Sci.*, 2014, **317**, 511–516, DOI: 10.1016/j.apsusc.2014.08.141.

38 Y. Inada and H. Orita, Efficiency of numerical basis sets for predicting the binding energies of hydrogen bonded complexes: evidence of small basis set superposition error compared to Gaussian basis sets, *J. Comput. Chem.*, 2008, **29**(2), 225–232, DOI: 10.1002/jcc.20782.

39 M. J. Ungerer, C. G. C. E. van Sittert, D. J. van der Westhuizen and H. M. Krieg, Molecular modelling of tantalum penta-halides during hydrolysis and oxidation reactions, *Comput Theor Chem*, 2016, **1090**, 112–119, DOI: 10.1016/j.comptc.2016.06.011.

40 B. Delley, The conductor-like screening model for polymers and surfaces, *Mol. Simul.*, 2006, **32**(2), 117–123, DOI: 10.1080/08927020600589684.

41 M. H. Opi, T. Ahmed, M. R. Swarna, A. A. Piya and S. U. D. Shamim, Assessment of the drug delivery potential of graphene, boron nitride and their in-plane doped structures for hydroxyurea anti-cancer drug *via* DFT study, *Nanoscale Adv.*, 2024, **6**(20), 5042–5054, DOI: 10.1039/d4na00428k.

42 M. Shahabi and H. Raissi, Investigation of the solvent effect, molecular structure, electronic properties and adsorption mechanism of Tegafur anticancer drug on Graphene nanosheet surface as drug delivery system by molecular dynamics simulation and density functional approach, *J. Inclusion Phenom. Macrocyclic Chem.*, 2017, **88**(3–4), 159–169, DOI: 10.1007/s10847-017-0713-9.

43 S. N. Ema, M. A. Khaleque, A. Ghosh, A. A. Piya, U. Habiba and S. U. D. Shamim, Surface adsorption of nitrosourea on pristine and doped (Al, Ga and In) boron nitride nanosheets as anticancer drug carriers: The DFT and COSMO insights, *RSC Adv.*, 2021, **11**(58), 36866–36883, DOI: 10.1039/d1ra07555a.

44 J. Mawwa, S. U. D. Shamim, S. Khanom, M. K. Hossain and F. Ahmed, In-plane graphene/boron nitride heterostructures and their potential application as toxic gas sensors, *RSC Adv.*, 2021, **11**(52), 32810–32823, DOI: 10.1039/d1ra06304a.

45 R. Ziraoui, H. Meghraoui, M. El Gouri, M. Rafik and A. Elharfi, Synthesis and physico chemical study of a new hexa and tetra functional epoxy materials based on bis -para-terephthalylidene phosphoric ester, *J. Mater. Environ. Sci.*, 2010, **1**(4), 213–218.

46 M. Franco-Pérez, C. A. Polanco-Ramírez, J. L. Gázquez and P. W. Ayers, Local and nonlocal counterparts of global descriptors: the cases of chemical softness and hardness, *J. Mol. Model.*, 2018, **24**(10), 285, DOI: 10.1007/s00894-018-3823-4.

47 M. Abolmaesoomi, A. Abdul Aziz, S. Mat Junit and J. Mohd Ali, Ficus deltoidea: Effects of solvent polarity on antioxidant and anti-proliferative activities in breast and colon cancer cells, *Eur. J. Intern. Med.*, 2019, **28**, 57–67, DOI: 10.1016/j.eujim.2019.05.002.

48 C. Wang, L. Shen and L. Wu, Adsorption and sensing of an anticancer drug on the boron nitride nanocones; a computational inspection, *Comput Methods Biomech*

Biomed Engin, 2021, **24**(2), 151–160, DOI: 10.1080/10255842.2020.1815716.

49 S. Benabid, Y. Benguerba, I. M. AlNashef and N. Haddaoui, Theoretical study of physicochemical properties of selected ammonium salt-based deep eutectic solvents, *J. Mol. Liq.*, 2019, **285**, 38–46, DOI: 10.1016/j.molliq.2019.04.052.

50 N. Sharma, R. Kakkar, P. Bansal, *et al.*, Host–guest complexation studies of p-tertbutylcalix[4]arene against ions of interest for radiological decontamination, *Inorg. Chim. Acta*, 2019, **484**, 111–124, DOI: 10.1016/j.ica.2018.09.007.